New Developments in Data for Auger Electron Spectroscopy and X-ray Photoelectron Spectroscopy

C. J. Powell[1*], A. Jablonski[2], F. Salvat[3], S. Tanuma[4], and D. R. Penn[1]

[1]*National Institute of Standards and Technology, Gaithersburg, MD 20899-8370, USA*

[2]*Institute of Physical Chemistry, ul. Kasprzaka 44/52, 01-224 Warsaw, Poland*

[3]*Facultat de Fisica (ECM), Universitat de Barcelona, Diagonal 647, 08028 Barcelona, Spain*

[4]*National Institute for Materials Science, 1-2-1 Sengen, Tsukuba 305-0047, Japan*

*cedric.powell@nist.gov

A brief description is given of three recent developments concerning the generation and application of data for elastic and inelastic scattering of electrons relevant to Auger-electron spectroscopy (AES) and X-ray photoelectron spectroscopy. First, an extensive analysis of calculated and measured differential cross sections for elastic scattering of electrons by atoms has been published. Second, new calculations have been made of electron inelastic mean free paths for additional solids. Third, new Monte Carlo simulations of electron backscattering relevant to AES have been performed that make use of the most-up-to-date values of the relevant cross sections. Calculated values of electron backscattering factors for four illustrative Auger transitions and energies between 3 keV and 10 keV agree reasonably with values from Shimizu's empirical formula for normal incidence. Values of the information radius for a copper film on silicon and gold substrates have been obtained at energies of 5 keV and 10 keV.

INTRODUCTION

Data for key physical parameters are needed for surface analyses by Auger-electron spectroscopy (AES) and X-ray photoelectron spectroscopy (XPS). These applications include identification of chemical state from chemical shifts of Auger-electron and photoelectron lines, correction of matrix effects in quantitative AES and XPS analyses, and measurements of overlayer-film thicknesses. Data describing elastic and inelastic scattering of the incident electrons (in AES) and of the signal electrons (in AES and XPS) are also needed for modeling the electron transport, particularly for inhomogeneous specimens.

The National Institute of Standards and Technology (NIST) currently offers four databases for applications in surface analysis and surface science [1-5]. These databases are intended principally for use with AES and XPS but are also useful for other surface-sensitive spectroscopies in which electron beams are employed, for other

analytical applications such as electron-probe microanalysis and analytical electron microscopy, and for other purposes such as electron-beam lithography and radiation physics. The four databases are:

- NIST X-Ray Photoelectron Spectroscopy Database (SRD 20)
- NIST Electron Elastic-Scattering Cross-Section Database (SRD 64)
- NIST Electron Inelastic-Mean-Free-Path Database (SRD 71)
- NIST Electron Effective-Attenuation-Length Database (SRD 82)

The XPS database is available on the internet [5] while the other three databases operate on personal computers [4]. Three extensive review articles have been published that discuss the relevant concepts, theoretical and experimental methods, and data reliability for SRD 64 [6], SRD 71 [7], and SRD 82 [8].

We present brief accounts of three recent developments in the provision of data for AES and XPS. First, we describe a recent analysis of calculated and measured differential cross sections for elastic scattering of electrons by atoms. Second, we report on new calculations of electron inelastic mean free paths for additional solids. Finally, we describe some results of new Monte Carlo simulations of electron backscattering in AES that make use of the most up-to-date values of the relevant cross sections for elastic and inelastic scattering.

DIFFERENTIAL CROSS SECTIONS FOR ELASTIC SCATTERING OF ELECTRONS BY ATOMS

A detailed analysis has recently been published [6] of calculated differential cross sections (DCSs) for elastic scattering of electrons by atoms from the Dirac-Hartree-Fock (DHF) potential (as now given in Version 3.1 of NIST SRD 64 [4]) and of similar cross sections from the Thomas-Fermi-Dirac (TFD) potential (as previously given in Versions 1.0 and 2.0 of SRD 64). DCSs from the former potential are believed to be more accurate than those from the latter potential, and measured DCSs generally agree better with cross sections calculated from the DHF potential although there are increasing deviations for energies less than 1 keV. These deviations can be accounted for by corrections for polarization and absorption effects at small and large scattering angles, respectively [9]. Nevertheless, atomic cross sections for elastic scattering without these corrections have been successfully used in Monte Carlo simulations of signal-electron transport in AES and XPS and similar applications for energies larger than about 300 eV [6, 10].

Values of electron inelastic mean free paths (IMFPs) have been derived from measurements of elastic-backscattered probabilities, a technique known as elastic-peak electron spectroscopy (EPES) [7, 11]. Most commonly, relative measurements are made under the same conditions of the intensities of elastically backscattered electrons from two surfaces,
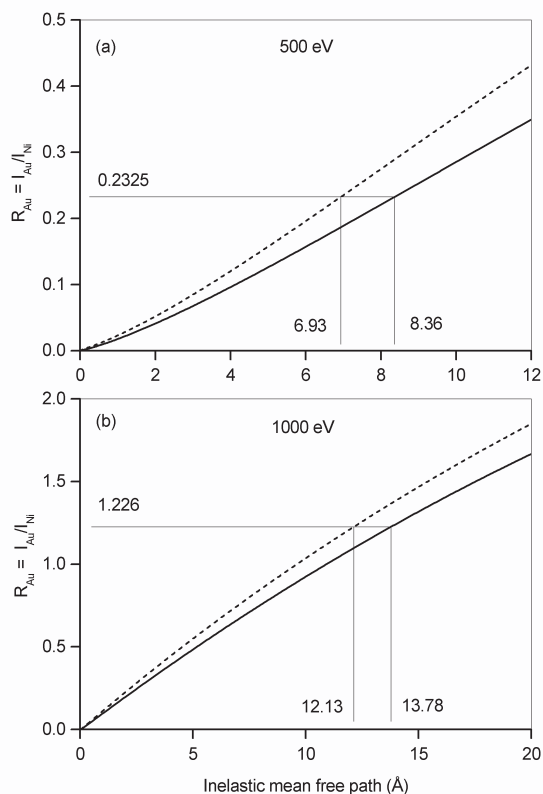

Fig. 1. Ratio of elastic-backscattering probabilities $R_{Au} = I_{Au}/I_{Ni}$ for an EPES experiment with an Au specimen and a Ni standard as a function of assumed values of the IMFP of Au for the experimental configuration of Jablonski *et al.* [12, 13]. The solid lines show calibration curves obtained with DCSs from the DHF potential and the dashed line shows these curves with DCSs from the TFD potential for electron energies of (a) 500 eV and (b) 1000 eV [6].

one the specimen of interest and the other a "standard" material for which the IMFP is considered to be sufficiently well known. Ratios of the same intensities are also calculated from a suitable theoretical model describing the backscattering phenomenon. In these calculations, atomic DCSs (e.g., from SRD 64) are used to describe elastic scattering in the specimen and standard materials for the energies of interest, and the specimen IMFP is considered a variable parameter. So-called calibration curves are produced in which the ratio R of the elastic-backscattering probabilities is plotted as a function of the specimen IMFP for the relevant experimental configuration. By comparison of the measured and calculated intensity ratios, the IMFP of the specimen can be determined.
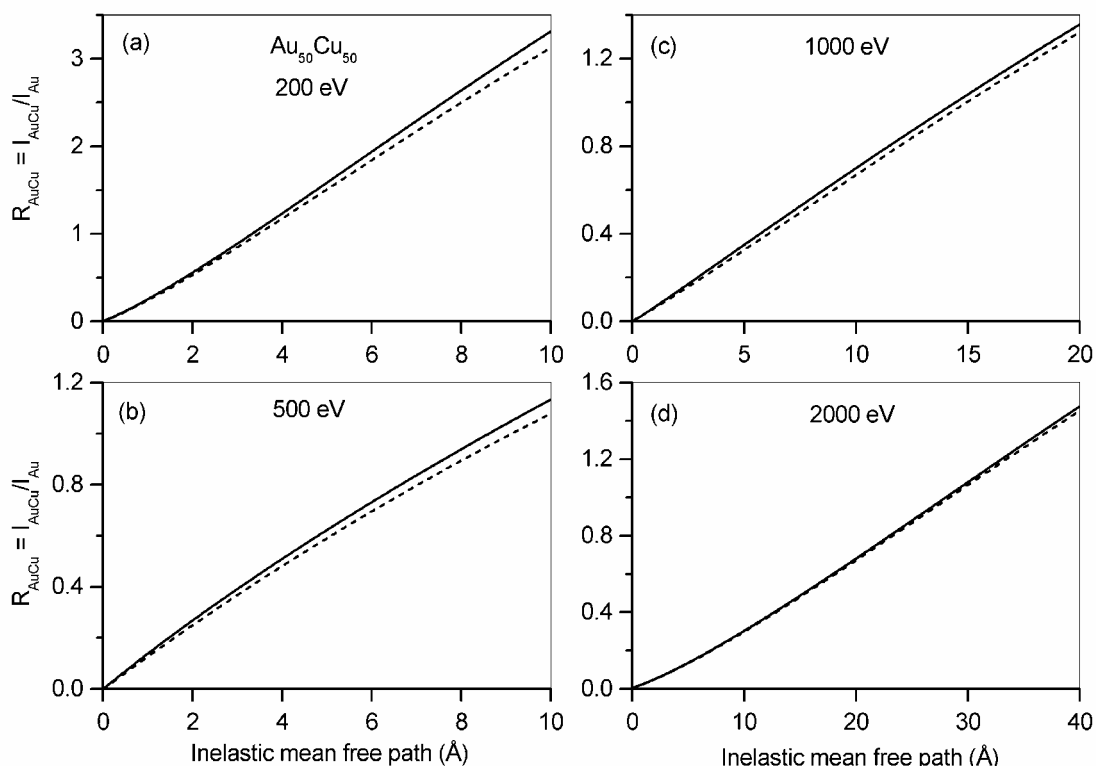
Fig. 2. Ratio of elastic-backscattering probabilities $R_{AuCu} = I_{AuCu} / I_{Aui}$ for an EPES experiment with an AuCu specimen and an Au standard as a function of assumed values of the IMFP of AuCu for the experimental configuration of Krawczyk *et al.* [14]. The solid lines show calibration curves obtained with DCSs from the DHF potential and the dashed line shows these curves with DCSs from the TFD potential for electron energies of (a) 200 eV, (b) 500 eV, (c) 1000 eV, and (d) 2000 eV [6].

We now consider the extent to which the calibration curves for EPES may vary depending on whether the DCSs for elastic scattering were computed from the TFD or DHF potentials. Figure 1 shows calibration curves [6] for these potentials for the case of a gold specimen, a nickel standard, electron energies of 500 eV and 1000 eV, and an experimental configuration in which the mean scattering angle was 155° [12, 13]. In this example, a deep minimum in the DCS for gold occurs in the vicinity of this scattering angle, and there are appreciable differences in the DCSs from the two potentials [6]; smaller differences occur at 1000 eV. If the measured ratio $R_{Au} = I_{Au} / I_{Ni}$ is assumed to be 0.2325 at 500 eV and 1.226 at 1000 eV (these values correspond to the "recommended IMFPs" for gold of 8.36 Å and 13.78 Å at these energies, respectively [7]), then there will be corresponding differences in the derived IMFPs of −17.1 % and −

12.0 % if the calibration curves were obtained with DCSs from the TFD potential. This example is thought to be a "worst-case" situation. Figure 2 shows similar calibration curves [6] for EPES experiments with an AuCu sample, an Au standard, and an experimental configuration for which the mean scattering angle was 138° [14]. In this case, the differences in derived IMFPs from calibration curves for the two potentials range from 1.3 % to 5.8 % for the measured intensity ratios at the four energies [6].

NEW CALCULATIONS OF ELECTRON IMFPs

Tanuma *et al.* [15-17] have reported calculations of IMFPs for 50 eV to 2000 eV electrons from experimental optical data for 27 elemental solids, 15 inorganic compounds, and 14 organic compounds. These authors analyzed the IMFPs for the groups of elemental solids and organic compounds to derive an

equation, designated TPP-2M [17], based on the Bethe equation for inelastic scattering of electrons in matter [18]. The TPP-2M equation is:

$$\lambda = E / \{E_p^2[\beta \ln(\gamma E) - (C/E) + (D/E^2)]\} \tag{1a}$$

$$\beta = -0.10 + 0.944/(E_p^2 + E_g^2)^{0.5} + 0.069\rho^{0.1} \tag{1b}$$

$$\gamma = 0.191\rho^{-0.5} \tag{1c}$$

$$C = 1.97 - 0.91U \tag{1d}$$

$$D = 53.4 - 20.8U \tag{1e}$$

$$U = N_v\rho/M = E_p^2/829.4 \tag{1f}$$

where λ is the IMFP (in Å), E the electron energy (in eV), $E_p = 28.8(N_v\rho/M)^{1/2}$ is the free-electron plasmon energy (in eV), N_v is the number of valence electrons per atom or molecule, ρ is the bulk density (in g cm^{-3}), M is the atomic or molecular weight, and E_g is the band-gap energy for non-conductors. The average root-mean-square (RMS) deviations between IMFPs from eq. (1) and IMFPs from optical data were 10.2 % and 8.5 % for the groups of elements and organic compounds, respectively [17]. These deviations were considered acceptable given the empirical nature of eq. (1) and the uncertainties of the optical data from which the IMFPs were calculated. The TPP-2M equation could then be used to estimate IMFPs in other solids [17].

Tanuma *et al.* have now made additional IMFP calculations [19] for an additional 14 elemental solids (Li, Be, diamond, graphite, Na, K, Sc, Ge, In, Sn, Cs, Gd, Tb, and Dy) and for one solid (Al) using better optical data than in the earlier work [15]. While IMFPs from the TPP-2M equation agreed adequately with the calculated IMFPs for most of the additional solids, there were surprisingly large RMS deviations for diamond (71.8 %), graphite (49.5 %), and cesium (39.3 %). As an example, Fig. 3 shows a plot of the IMFPs for diamond obtained from optical data (solid circles) and IMFPs from TPP-2M (dashed line).
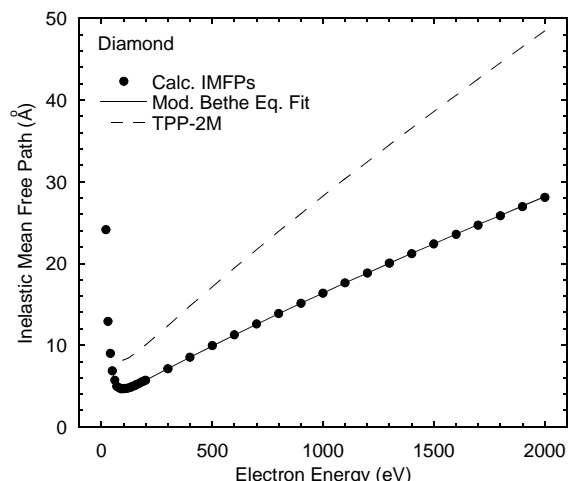

Fig. 3. MFPs (solid circles) calculated for diamond as a function of electron energy [19]. The solid line is a fit to the modified Bethe equation [Eq. (1a) with β, γ, C, and D allowed to vary]. The dashed line shows IMFPs calculated from the TPP-2M predictive formula [Eq. (1)].

Analysis showed that the large RMS deviations occurred for extreme values of the parameter β in the TPP-2M equation [19]. When the calculated value of β is small (~ 0.01), as it is for diamond and graphite, the relative uncertainty of β can be large. When the calculated value of β is large (~ 0.25), as it is for Cs, the TPP-2M equation does not provide reliable IMFPs. Fortunately, for current applications, there seem to be few materials for which such extreme values of β will be encountered. Unfortunately, the lack of materials with these extreme values of β makes it difficult to derive empirical modifications of Eq. 1(b) for such situations.

Tanuma *et al.* recently discussed the appropriate choice of the parameter N_v in TPP-2M [20]. For most elements, they recommended that N_v be calculated from the number of valence electrons per atom in a given solid. For the rare-earth elements, however, they recommended that N_v be computed from the sum of the number of valence electrons in the solid state (either two or three) and the six 5p electrons that have binding energies between 18 eV and 27 eV [19]. Due to a resonance excitation, the 5p electrons contribute strongly to the energy-loss function and to the IMFP.
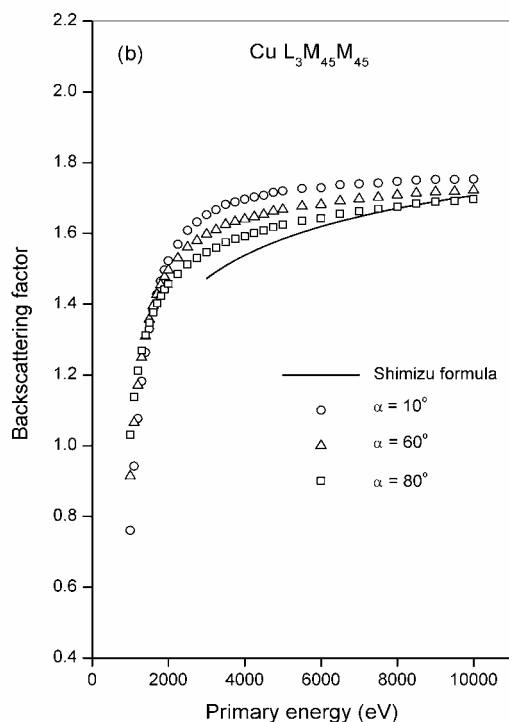
Fig. 4. The symbols show calculated backscattering factors for Cu $L_3M_{45}M_{45}$ Auger electrons as a function of primary energy for normal incidence of the primary beam and for values of the Auger-electron emission angle, α, of 10° (circles), 60° (triangles), and 80° (squares) [25]. The solid line shows BFs from the Shimizu [24] formula [Eq. (2)].

In contrast, the 4f electrons contribute weakly to the energy-loss function and IMFP. The same rationale indicates that the six 5p electrons of Cs should be included in the count for N_v; this choice, however, does not significantly reduce the RMS deviation between IMFPs from TPP-2M and those from optical data [19]. Experimental IMFP measurements are needed to test whether the ten 4d electrons should be included in the count of N_v for elements such as In and Sn since these electrons also contribute strongly to the energy-loss function [19].

MONTE CARLO SIMULATIONS OF ELECTRON BACKSCATTERING FOR AES

The backscattering factor (BF) is needed for quantitative analyses by AES [21]. An extensive database of BFs was published by Shimizu and

Ichimura [22] and Ichimura and Shimizu [23]. These values were obtained from Monte Carlo (MC) simulations of electron transport in solids performed for numerous primary-electron energies between 3 keV and 10 keV, three angles of primary-beam incidence, and many elemental solids and binary compounds. Shimizu [24] later derived useful empirical expressions for the BF, r_{BF}, as a function of the atomic number Z (or average atomic number for a compound) and the ratio U_0 of the primary energy E_0 to the binding energy E_c of the core level responsible for the Auger transition of interest. For normal incidence of the primary beam on the sample, Shimizu's expression is:

$$r_{BF} = 1 + (2.34 - 2.10Z^{0.14})\,U_0^{-0.35} + (2.58Z^{0.14} - 2.98) \tag{2}$$

Similar expressions were derived for incidence angles of 30° and 45° [24].

Jablonski and Powell [25] have performed a new series of MC simulations to calculate BFs for illustrative Auger transitions in four elemental solids (Si $KL_{23}L_{23}$, Cu $L_3M_{45}M_{45}$, Ag $M_5N_{45}N_{45}$, and Au $M_5N_{45}N_{45}$). These simulations were performed with a new algorithm that is not based on the assumption of the probability of inner-shell ionization being independent of depth [26]. Scattering and ionization cross sections of the highest reliability were selected. Differential cross sections for elastic scattering were obtained from the DHF potential (rather than the TFD potential used by Shimizu and Ichimura), inner-shell ionization cross sections were obtained from the empirical formula of Casnati *et al.* [27] (rather than the Gryzinski formula [28] used by Shimizu and Ichimura), and inelastic scattering was described by energy-loss functions from experimental optical data [15, 19] and IMFPs from fits to calculated IMFPs from 50 eV to 10 keV [7] (rather than the Bethe stopping power [18] used by Shimizu and Ichimura). The new simulations were performed for primary-electron energies between 0.5 keV and 10 keV, normal incidence of the primary beam, and Auger electrons emitted at angles between 10° and 80° with respect to the surface normal.
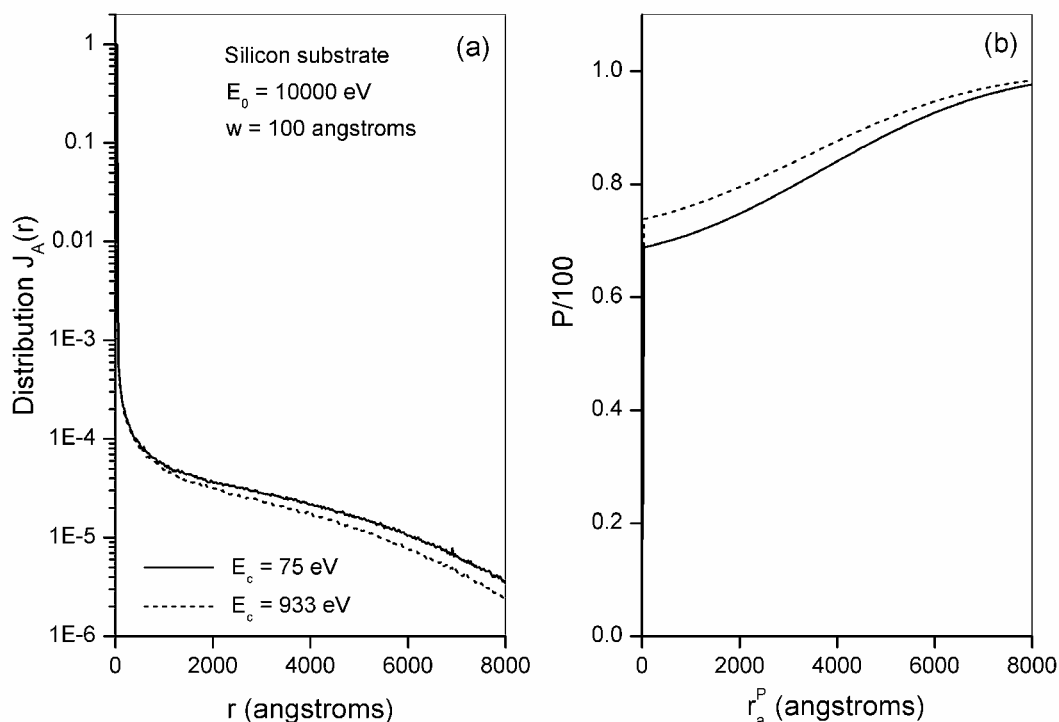
Fig. 5 a) Radial distribution of the Cu Auger-electron intensity, $J_A(r)$ for a thin copper film on a silicon substrate and with a primary energy of 10,000 eV. (b) The fractional intensity, I/I_{max}, as a function of the integration radius r_a^P calculated from Eq. (3). Solid line: Cu M_3VV Auger electrons; dashed line: Cu $L_3M_{45}M_{45}$ Auger electrons [29].
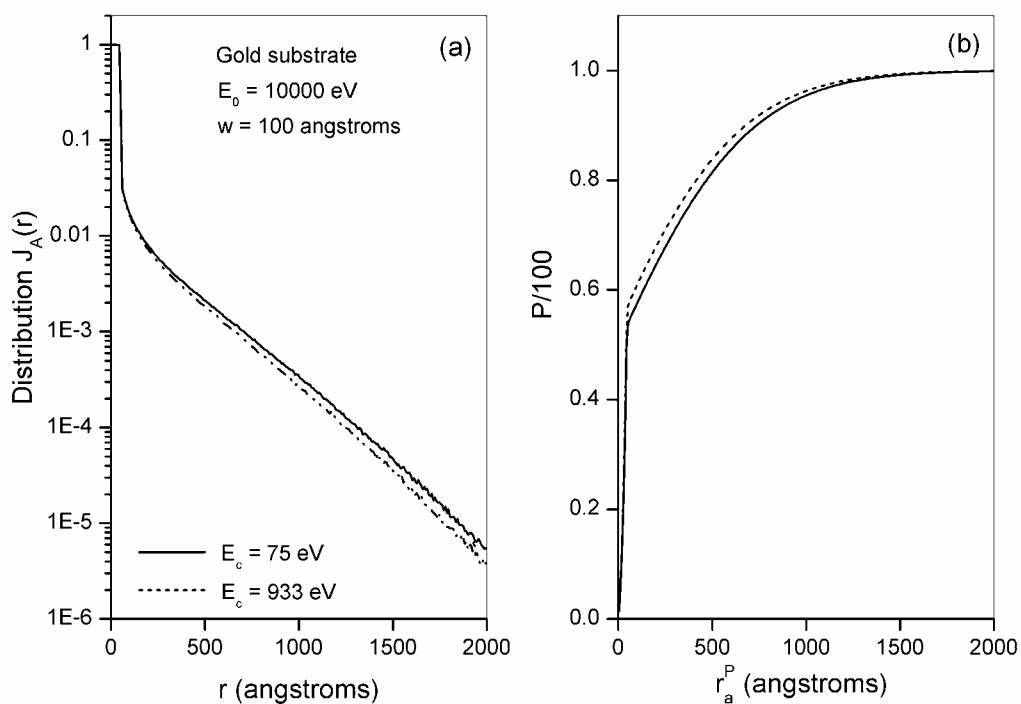

Fig. 6 a) Radial distribution of the Cu Auger-electron intensity, $J_A(r)$ for a thin copper film on a gold substrate and with a primary energy of 10,000 eV. (b) The fractional intensity, I/I_{max}, as a function of the integration radius r_a^P calculated from Eq. (3). Solid line: Cu M_3VV Auger electrons; dashed line: Cu $L_3M_{45}M_{45}$ Auger electrons [29].

As an example of the new BF results [25], Fig. 4 shows the calculated BFs (symbols) for Cu $L_3M_{45}M_{45}$ Auger electrons as a function of primary energy for three values of the Auger-electron emission angle, α. We see that there is a weak dependence of the BF on α, a new result. The calculated BFs are generally larger in this example than BFs from Eq. (2) (the solid line) but show a similar dependence on primary energy. For the other three solids, the calculated BFs are also generally larger than values from Eq. (2) for Au $M_5N_{67}N_{67}$ Auger electrons, are smaller than BFs from Eq. (2) for Ag $M_5N_{45}N_{45}$ Auger electrons, and both smaller and larger for Si $KL_{23}L_{23}$ Auger electrons. Overall, the new BFs agreed with values from Eq. (2) to better than 11 %. At primary energies close to the threshold energy for inner-shell ionization, the BF is less than unity because the probability of inner-shell ionization is varying substantially with depth [25, 26].

Jablonski and Powell [29] have investigated the effects of backscattered electrons in scanning Auger microscopy (SAM) on the radial distributions of emitted Auger electrons. They considered the emission of Cu $M_3M_{45}M_{45}$ and $L_3M_{45}M_{45}$ Auger electrons from a thin Cu overlayer on a substrate of Si or Au for primary electrons with energies of 5 keV and 10 keV that were normally incident on the sample. The Cu layer was assumed to be sufficiently thin that there were no changes in the angular and energy distributions of primary and backscattered electrons passing through the overlayer. For simplicity, the primary beam was assumed to have a uniform current density and a width, w, of 100 Å.

Figures 5(a) and 6(a) show the radial distributions of the Cu Auger electrons, $J_A(r)$, excited by 10 keV primary electrons for substrates of Si and Au, respectively [29]. The solid lines show the radial distributions for the Cu $M_3M_{45}M_{45}$ Auger electrons (with a threshold energy, E_c, of 75 eV for ionization of the M_3 subshell) while the dashed lines show similar distributions for the Cu $L_3M_{45}M_{45}$ Auger electrons (where E_c is 933 eV for ionization of the L_3 subshell). We see that there is very little difference in the radial distributions for the two Cu Auger transitions, despite the order of magnitude difference in the values of E_c.

It is useful to determine the information radius, r_a^P, of the area from which a selected percentage P of the emitted Auger-electron signal originates. Powell [30] has proposed that r_a^P be defined in a similar way as the information depth in AES and XPS [31] to provide a useful measure of the analysis area in SAM. Values of r_a^P can be obtained by solving the following equation,

$$\frac{I}{I_{max}} = \frac{\int_0^{r_a^P} 2\pi \, r \, J_A(r) \, dr}{\int_0^{\infty} 2\pi \, r \, J_A(r) \, dr} = \frac{P}{100}, \qquad (3)$$

after selecting a desired value of P. For example, if P was chosen to be 80, 90, or 95, we can use Eq. (3) to determine the radius of the area from which 80 %, 90 %, or 95 %, respectively, of the Auger signal is emitted.

Figures 5(b) and 6(b) show plots of I/I_{max}, the ratio of the Auger intensity emitted within the radius r_a^P to the total emitted Auger intensity from Eq. (3), as a function of r_a^P for substrates of Si and Au, respectively. While approximately 70 % of the total Auger intensity for the Si substrate and approximately 55 % of the total Auger intensity for the Au substrate is emitted from within a radius of 50 Å (the radius of the primary beam), the remaining intensity is emitted from a much larger area. For example, if P is selected to be 90, then values of r_a^P range from 4602 Å to 5313 Å for Cu $L_3M_{45}M_{45}$ and $M_3M_{45}M_{45}$ Auger electrons, respectively, with the Si substrate, and from 678 Å to 736 Å, respectively, with the Au substrate. These results indicate that backscattered electrons can significantly increase the information radius in SAM, as found recently from use of a simplified model [30]. A "point" analysis by SAM of a selected small feature will generally lead to Auger signals from the nearby matrix as well as from the feature of interest.

SUMMARY

An overview has been presented of three recent developments in the development of data for AES and XPS. First, an extensive analysis has been recently made of calculated and measured differential cross sections for elastic scattering of electrons by

atoms [6]. This analysis showed that differential cross sections calculated from the Dirac-Hartree-Fock potential were more reliable than those from the Thomas-Fermi-Dirac potential. Since cross sections from the latter potential have frequently been used to model the transport of elastically backscattered electrons in EPES experiments to determine IMFPs, an examination was made of the extent to which the derived IMFPs depended on the potential used in the cross-section calculations. In one example, believed to be a "worst-case" situation, there was a 17.1 % change of the derived IMFPs while the change was less than 6 % for another example.

Second, new calculations of IMFPs have been made of electron IMFPs for an additional 14 elemental solids for electron energies from 50 eV to 2000 eV [19]. The calculated IMFPs for diamond and graphite differed appreciably from IMFPs derived from the TPP-2M IMFP predictive formula. These deviations were attributed to a limitation of the TPP-2M formula when one parameter (β) reached extreme values.

Finally, new Monte Carlo simulations of electron backscattering in AES have been made with what are believed to be the most reliable values of the relevant scattering and ionization cross sections [25, 29]. Values of the backscattering factor for illustrative Auger transitions in Si, Cu, Ag, and Au for primary-electron energies between 3 keV and 10 keV and normal incidence agreed to better than 11 % with values from the empirical formula developed by Shimizu some twenty years ago [24]. In scanning Auger microscopy, the information radius for the detected signal can be appreciably larger than the radius of the primary beam used to locate a fine feature. In such cases, account should be taken of the Auger signal associated due to excitations by backscattered electrons in the nearby matrix.

ACKNOWLEDGMENT

REFERENCES

[1] C. J. Powell, A. Jablonski, A. Naumkin, A. Kraut-Vass, J. M. Conny, and J. R. Rumble, Jr., J. Electron Spectrosc. Relat. Phenom. **114-116**, 1097 (2001).

[2] C. J. Powell and A. Jablonski, J. Surf. Anal. **9**, 322 (2002).

[3] C. J. Powell and A. Jablonski, J. Surf. Anal. 10, 158 (2003).

[4] Further information on the NIST databases can be obtained from: http://www.nist.gov/srd/surface.

[5] The NIST XPS Database can be accessed at: http://srdata.nist.gov/xps.

[6] A. Jablonski, F. Salvat, and C. J. Powell, J. Phys. Chem. Ref. Data 33, 409 (2004).

[7] C. J. Powell and A. Jablonski, J. Phys. Chem. Ref. Data 28, 19 (1999).

[8] A. Jablonski and C. J. Powell, Surf. Science Reports 47, 33 (2002).

[9] F. Salvat, Phys. Rev. A 68, 012708 (2003).

[10] A. Jablonski, F. Salvat, and C. J. Powell, J. Electron Spectrosc. Rel. Phenom. 137-140, 299 (2004).

[11] G. Gergely, Prog. Surf. Science 71, 31 (2002).

[12] A. Jablonski, H. S. Hansen, C. Jansson, and S. Tougaard, Phys. Rev. B 45, 3694 (1992).

[13] A. Jablonski, J. Zemek, and P. Jiricek, Surf. Interface Anal. 31, 825 (2001).

[14] M. Krawczyk, L. Zommer, A. Jablonski, C. Robert, J. Pavluch, L. Bideux, and B. Gruzza, Surf. Interface Anal. 31, 415 (2001).

[15] S. Tanuma, C. J. Powell, and D. R. Penn, Surf. Interface Anal. 17, 911 (1991).

[16] S. Tanuma, C. J. Powell, and D. R. Penn, Surf. Interface Anal. 17, 927 (1991).

[17] S. Tanuma, C. J. Powell, and D. R. Penn, Surf. Interface Anal. 21, 165 (1994).

[18] H. Bethe, Ann. Physik 5, 325 (1930).

[19] S. Tanuma, C. J. Powell, and D. R. Penn, Surf. Interface Anal. 37, 1 (2005).

[20] S. Tanuma, C. J. Powell, and D. R. Penn, Surf. Interface Anal. 35, 268 (2003).

[21] H. E. Bishop and J. C. Riviere, J. Appl. Phys. 40, 1740 (1969).

[22] R. Shimizu and S. Ichimura, Quantitative Analysis by Auger Electron Spectroscopy, Toyota Foundation Research Report No. I-006 76-0175, Tokyo, 1981.

[23] S. Ichimura and R. Shimizu, Surf. Science 112, 386 (1981).

[24] R. Shimizu, Japanese J. Appl. Phys. 22, 1631 (1983).

[25] A. Jablonski and C. J. Powell, Surf. Science 574, 219 (2005).

[26] A. Jablonski, Surf. Science 499, 219 (2002).

[27] E. Casnati, A. Tartari, and C. Baraldi, J. Phys. B 15, 155 (1982).

[28] M. Gryzinski, Phys. Rev. 138, A336 (1965).

[29] A. Jablonski and C. J. Powell Appl. Surf. Science 242, 220 (2005).

[30] C. J. Powell, Appl. Surf. Science 230, 327 (2004).

[31] A. Jablonski and C. J. Powell, J. Vac. Sci. Tech. A 21, 274 (2003).